Journal of the Korean Astronomical Society
53: 1 ∼ 7, 2020 February

https://doi.org/10.5303/JKAS.2020.53.1.1
pISSN: 1225-4614 · eISSN: 2288-890X
http://jkas.kas.org

A Study of Small Flares Associated with Plasma Blobs Outflowing along Post-CME Rays

Yoo Jung Kim[1], Ryun-Young Kwon[2], and Jongchul Chae[1]

[1]Department of Physics and Astronomy, Seoul National University, Gwanak-gu, Seoul 08826, Korea; jcchae@snu.ac.kr
[2]Solar and Space Weather Group, Korea Astronomy and Space Science Institute, Daejeon, Korea

Received October 7, 2019; accepted December 20, 2019

Abstract: The recent study of Chae et al. (2017) found a one-to-one correspondence between plasma blobs outflowing along a ray formed after a coronal mass ejection (CME) and small X-ray flares. In the present work, we have examined the spatial configuration and the eruption process of the flares that are associated with the blobs by analyzing EUV images and magnetograms taken by the SDO/AIA and HMI. We found that the main flare and the successive small flares took place in a quadrupolar magnetic configuration characterized by predominant magnetic fields of positive polarity, two minor magnetic fragments of negative polarity, and a curved polarity inversion line between them, which suggests that the formation process of the blobs may be similar to that of the parent CME. We also found that the successive flares resulted in a gradual change of the quadrupolar magnetic configuration, and the relevant migration of flaring kernels. The three-dimensional geometry and the property of the current sheet, that is often supposed to be embedded in an observed post-CME ray, seem to keep changing because of mutual feedback between the successive flares and the temporal change of the magnetic field configuration. Our results suggest that the observed post-CME rays may not reflect the characteristics of the current sheet responsible for the impulsive phase of the flare.

Key words: magnetic reconnection — Sun: corona — Sun: flares — Sun: coronal mass ejections (CMEs)

1. Introduction

Bright rays (sometimes with blob-like features) are often observed a few hours after CME eruptions (Ko et al. 2003; Webb et al. 2003). These post-CME rays have been identified with the thin, long current sheets that are theoretically expected to form when CME occurs at a polarity inversion line (PIL) so that magnetic lines of reverse sign are open closely (Lin & Forbes 2000). The main difficulty of this identification is in the observed widths of the rays that are too big for the current sheets (Lin et al. 2015). An alternative view is to regard a post-CME ray as the channel for outflows produced by magnetic reconnection (e.g. Chae et al. 2017). In this view, the current sheet where magnetic reconnection occurs is located in the low corona, below the altitude where post-CME rays are observed in the coronagraphic images.

The three-dimensional geometry of a post-CME ray was examined in detail by Kwon et al. (2016). They studied two CMEs associated with two successive C-class flares observed on 21 September 2013 that were followed by several rays on the COR2 image of the STEREO Behind. It was found that the major ray was coaxial with the CME as expected, and had a cross section of $0.42\,R_\odot \times 1.24\,R_\odot$. The rays examined by Kwon et al. (2016) were all flowing outward as evidenced by the observable outward motion of plasma blobs along the rays.

Chae et al. (2017, Paper I hereafter) traced the blobs and other recognizable features seen in the same data as used by Kwon et al. (2016). They identified one CME front, one CME core, two ray tips, and 7 blobs from the STEREO COR2 Behind images taken for 40 hours of 21–22 September 2013, and determined their heights as functions of time. By extrapolating the height of each feature back in time, they estimated its departure time when the height was equal to the supposed initial height $0.5R_\odot$. As a result, they found that the departure times of the plasma blobs mostly coincided with the occurrence times of the corresponding small flares within 10 minutes. This coincidence is strong observational evidence that the ray represents outflowing material driven from the reconnecting current sheet.

The association of the plasma blobs with the small flares suggests that magnetic reconnection repeatedly occurs in the same current sheet formed by the CME eruption. This notion is compatible with numerical experiments of eruptions in two-dimensional magnetic configurations that reproduce a series of blobs as result of a tearing instability (see reviews by Lin et al. 2015; Webb & Vourlidas 2016). Therefore it is expected that the recurrent flares may have occurred in a similar way in similar magnetic configurations.

In this study, we investigate the development and magnetic configuration of the main flare and the subsequent small flares that are associated with the CME and the blobs studied by Chae et al. (2017), by examining the EUV images and magnetograms. This investigation allows us to correlate the blobs and outflows in the high

Corresponding author: J. Chae

Table 1
Features identified from the coronagraph observations and the EUV flares.

No.	Feature	Departure time (UT)	Ray no.	EUV flare	Peak time
1	CME front	2013-09-21 01:54			
2	CME core	2013-09-21 07:42			
3	Ray tip	2013-09-21 08:54	1	Main flare	09:22
4	Blob	2013-09-21 15:24	1	Separate flare	
5	Blob	2013-09-21 17:06	1	Subflare 1	17:17
6	Blob	2013-09-21 17:54	1	Subflare 2	17:37
7	Blob	2013-09-21 19:24	2	Subflare 3	19:44
8	Blob	2013-09-22 01:00	2	Subflare 4	00:45
9	Blob	2013-09-22 02:42	2	Subflare 5	02:46
10	Ray tip	2013-09-22 08:12	3	Subflare 6	08:00

corona region with the processes in the low corona region not only temporally but also spatially. Previously, there have been several studies of the low region of the current sheet (formed after CME) by observing in EUV or X-ray wavelengths (Forbes & Acton 1996; Lin et al. 2005; Savage et al. 2010). These studies showed the existence of structures like current sheets, cusp-shaped flare loops, and plasma inflows. However, no clear connection has been made yet between such phenomena in the low corona, and blobs observed in the high corona with coronagraphs.

2. DATA

In order to explore the EUV counterparts of the plasma outflows in coronagraphic images, we use the 131 Å and 1600 Å images of the Solar Dynamics Observatory (SDO; Pesnell et al. 2012) Atmospheric Imaging Assembly (AIA; Lemen et al. 2012) as well as magnetic field images taken by the Helioseismic and Magnetic Imager (HMI; Schou et al. 2012). The 131 Å images are sensitive to 4×10^5 K and 1×10^7 K corona plasma and hence can show the flare emission not only from very hot plasmas, but also from transition region temperature plasmas. The 1600 Å images show the upper part of the chromosphere and thus identify the footpoint of the loop. By making use of the flare emission from different temperature plasmas, we thus expect to reliably identify and compare the flare loops with the magnetic configurations.

We use the departure time of plasma outflows shown in Paper I. The departure times were determined under the assumption of constant acceleration, and they were found to be associated with small X-ray flares in the Geostationary Operational Environmental Satellite (GEOS) flux curve. Hence we investigate the EUV images taken around the departure times to search for the EUV signatures of the small X-ray flares as well as the plasma outflows observed in coronagraphic images.

3. RESULTS

Table 1 lists the coronagraph features and EUV flares we have identified in association with the moving features. The first flare was designated as "main flare" because it was a C-class major flare, and occurred in association with the second CME which was close to the first ray tip appearance. The small flares were designated as "subflares" because they occurred after the main flare and were B-class flares. Kwon et al. (2016) showed two flux rope structures expelled from the Sun, and Paper I confirmed there were, in fact, two flares associated with the two CMEs. Paper I traced two CME fronts, the CME core, two ray tips, and 7 blobs over two days from 21 to 22 September 2013. We re-examined the coronagraphic images and found another ray. Indeed, the post-CME ray is not a single structure but consists of at least three rays that are different in formation time, location, and orientation. Features 3–6 (ray tip and three blobs) shown in Figure 1 of Paper I belong to the first ray, features 7–9 (three blobs) to the second ray, and feature 10 to the last ray.

The difference between the departure times of the moving features and the flare peak times ranges from 4 min to 28 min (in the case of the main flare). This might be tolerable since the EUV flares last for 10 to 20 minutes.

Table 1 shows that the main flare occurred around 9:20 UT of September 21, 2013, in association with the ray tip (feature no. 3). Figure 1 shows that the flare occurred in AR11850 near the east limb. We also identified six small EUV flares associated with features 5 to 10, which are five blobs and one ray tip. All EUV counterparts of the main flare and the six small flares occurred in the same region marked by the orange box in Figure 1. We found another small flare around the time of feature 4 (blob), but it was found to be spatially separate. Thus we excluded this flare from our consideration, even though it occurred in the same active region. This is different from the procedure in Paper I where the EUV light curve was obtained from integrating the EUV light over the entire active region.

The right panel of Figure 1 shows a complex magnetic configuration, being far from a PIL as a straight line. The region is dominated by positive polarity (P1 and P2), and a curved PIL forms by the two negative magnetic fragments as marked by N1 and N2. As flares occurred repeatedly, the negative poles diminished, suggestive of collision-induced magnetic reconnection.

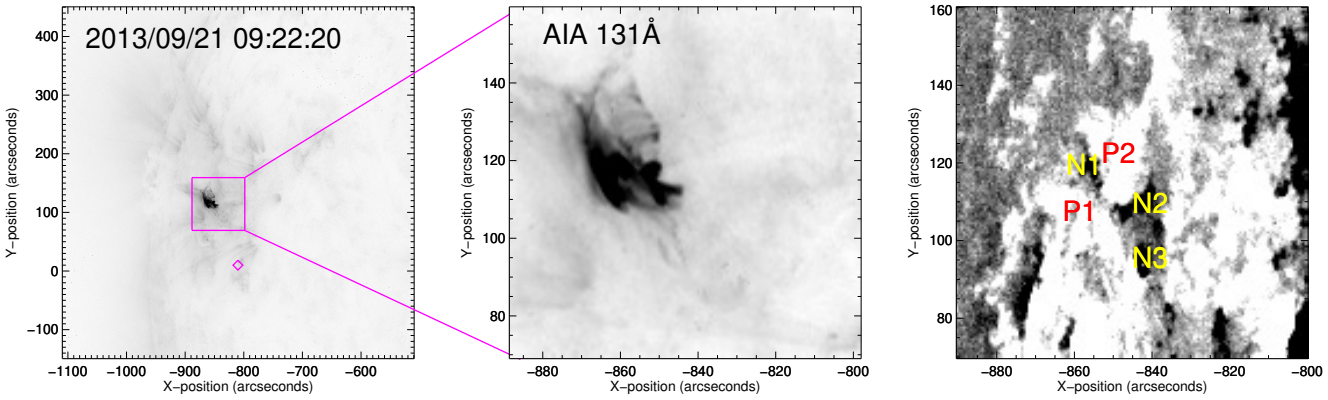

Figure 1. *Left:* The AIA 131 Å image of AR11850 taken on September 21, 2013 at the time of the main flare. The diamond marks the location of the flare associated with feature 4. *Center:* Magnified view of the region where the main flare occurred. *Right:* SDO/HMI line-of-sight magnetogram of the same region. The area where the magnetic field is entering is indicated in black, and the area coming out is indicated in white. The areas associated with the main flare are labeled P1, P2, N1, and N2.

3.1. Main Flare

Figure 2 shows images of the development of the main flare along the EUV light curves. Since all flares of interest occur within a small region, the light curves were obtained by integrating the intensities over the region each time, normalized by the median integrated intensity. The median integrated intensity is derived by taking the median value from the whole light curves from the onset of the main flare to the end of the last subflare. It is evident from the images that the PIL formed by the negative magnetic fragments marked by N1 and N2 is responsible for the flare. At Epoch A, the 1600 Å flare kernels first appeared in the four regions P1, P2, N1, and N2. The 131 Å loop connecting P2 and N2 appeared, and another loop connecting P1 and N2 showed up at Epoch B. At Epochs D and E, 1600 Å flare kernels of moderate strength occurred near P1 and N1, accompanying moderate 131 Å brightening. When the light curves appeared to be impulsive (Epoch F), two strong 1600 Å kernels are seen near P2 and N2, respectively, and a small, but very bright 131 Å loop connecting P2 and N2 showed up. Finally, around the peak time (Epoch G), strong flare kernels occurred at the regions P1, P2, N1, and N2.

3.2. Subflares

The subflares occurred in the same region as the main flare, and they developed with time in amanner similar to the main flare. Figure 3 presents the magnetic configuration and time development of the first three subflares. Subflare 1 was temporally associated with the second blob (see Table 1). It is the subflare most similar to the main flare, probably because the magnetic configuration did not change. It began with the appearance of a 131 Å loop connecting the 1600 Å kernels at P2 and N1 (Epoch (a) in Figure 3). At epoch (b), 1600 Å kernels occurred over the whole regions P1, P2, N1 and N2, while the light curves reach the peak. The two loops connecting P2–N1 and P2–N2, respectively, appeared.

Subflare 2 was temporally associated with the third blob. This flare was fainter than subflare 1, this flare loops cannot be distinguished. However, the flare kernels are identified at regions P1, P2, and N2. In addition, at epochs (e) and (f), a 131 Å loop connecting P2 to the western part appeared.

Subflare 3 was temporally associated with the fourth blob. It was brighter than subflares 1 and 2, thus the flare loop connecting the kernels on N1 and P2 can be identified clearly at Epoch (g). Loops connecting P2–N2 and P1–N2 are also observed. At Epoch (h), a bent loop connecting P2 and N2 developes and reaches its maximum flux at Epoch (i). This flare is similar to the main flare and the two preceding subflares in terms of morphological characteristics of flare kernels and loops.

Figure 4 presents the magnetic configuration and time development of the latter three subflares. Note that the magnetic configuration at the times of these flares were different from the one at the time of the main flare due to evolution with time. Nevertheless, the flaring region still maintained a quadrupolar configuration, so the subflares still appeared similar to the main flare. Subflare 4 was temporally associated with the fifth blob. At Epoch (a), a loop connecting P1 and N1 appeared. At Epoch (c), the flare kernel occurred at P2, and another loop connecting N1 to P2 was observed. This flare, however, appears different from the others in terms of location and its weak strength. Subflare 5 was temporally associated with the sixth blob. At Epoch (d), an arch-shaped eruption occurred at the regions of P1, N1, and P2. At Epoch (e), a very bright loop connecting P2 and N2 appeared. Finally, subflare 6 was temporally associated with the new ray tip. This flare is different from the main flare and the other subflares in terms of location of the kernels and flare loops. They occurred outside the original region of the quadrupolar configuration.

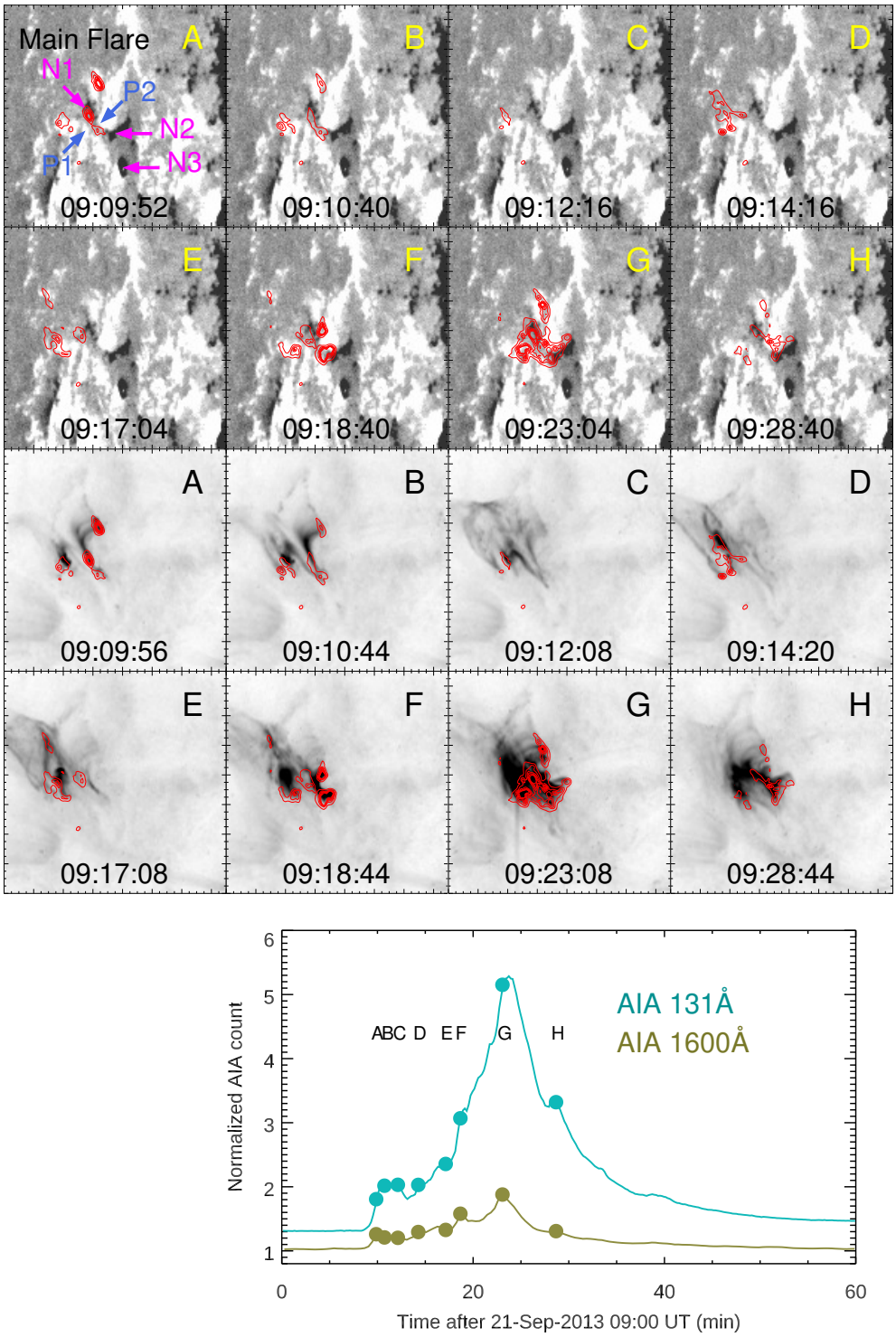

Figure 2. *Upper eight images:* SDO/HMI magnetograms at different epochs during the main flare. *Lower eight images:* AIA 131 Å images and AIA 1600 Å contours (in red) at the same epochs. *Bottom diagram:* The EUV light curves for the two wavelengths. Epochs A to H were marked in the curves for easy comparison with the corresponding images.

4. SUMMARY AND DISCUSSION

We investigated the EUV flares and their magnetic configuration from which the moving features in the coronagraph images originate. In Paper I, we traced features moving along post-CME rays which occurred on 21–22 September 2013 and found a one-to-one correspondence between the moving features and soft X-ray flares observed by the GOES satellite. The main flare was temporally associated with the first ray tip; the five blobs, with the five subflares, and the last subflare, were associated with the second ray tip.

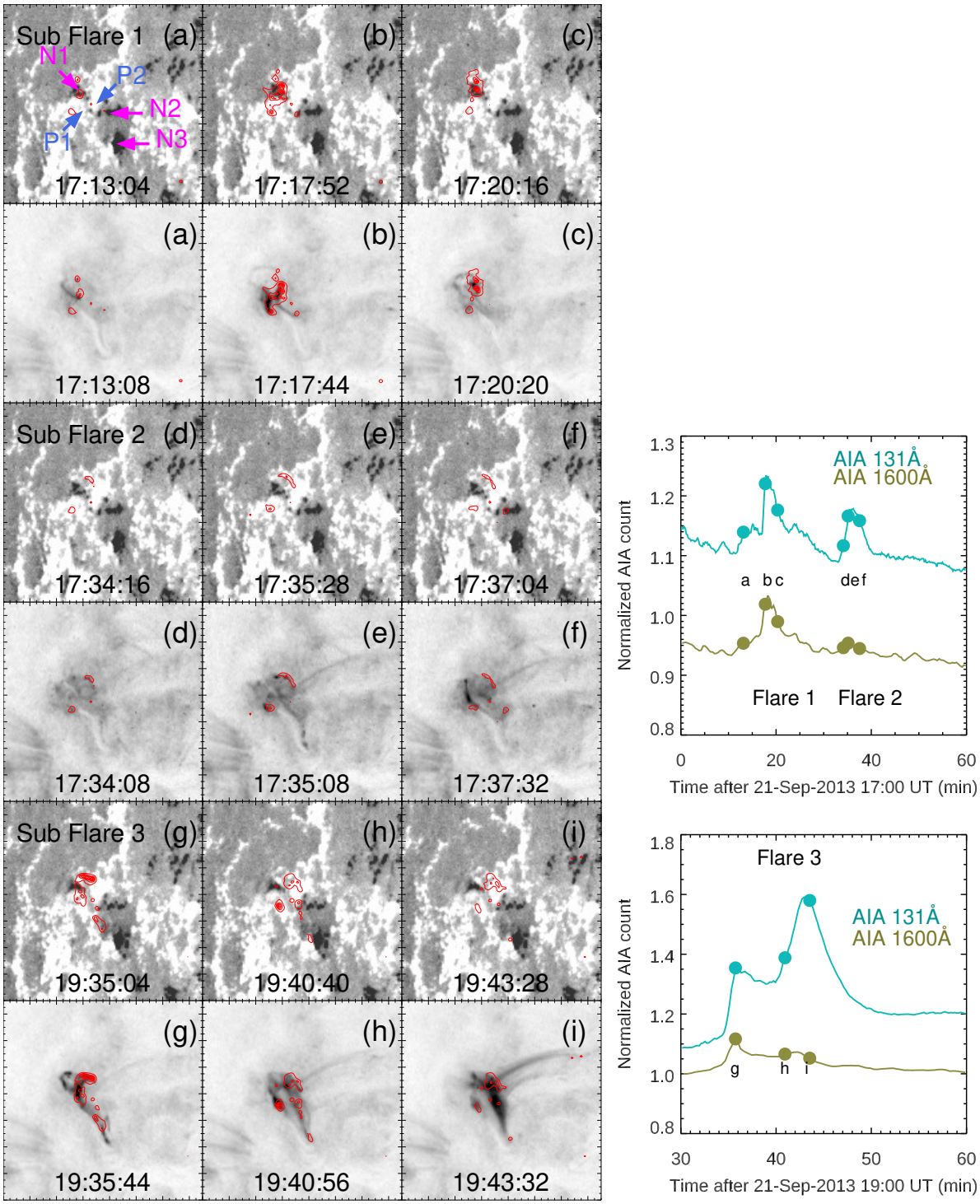

Figure 3. *Left:* Magnetograms and EUV images of subflares 1 to 3 at different epochs. *Right:* EUV light curves of the same flares.

In the present work, we located the GOES X-ray flares in the EUV images and projected the flare kernels onto magnetograms. We found that the subflares occurred in the same region of complex configuration as the main flare, and they developed with time in a manner similar to the main flare. The flaring region had a quadrupolar configuration composed of the dominant magnetic patches of positive polarity and two small magnetic fragments of negative polarity. These flares underwent similar temporal developments: flare kernels first occurred at two or three poles (designated N1, P1 and P2), and the flare loops connecting the kernels were visible, and later the flare kernels occurred at all the poles or the three poles (P1, P2 and N2). In addition,

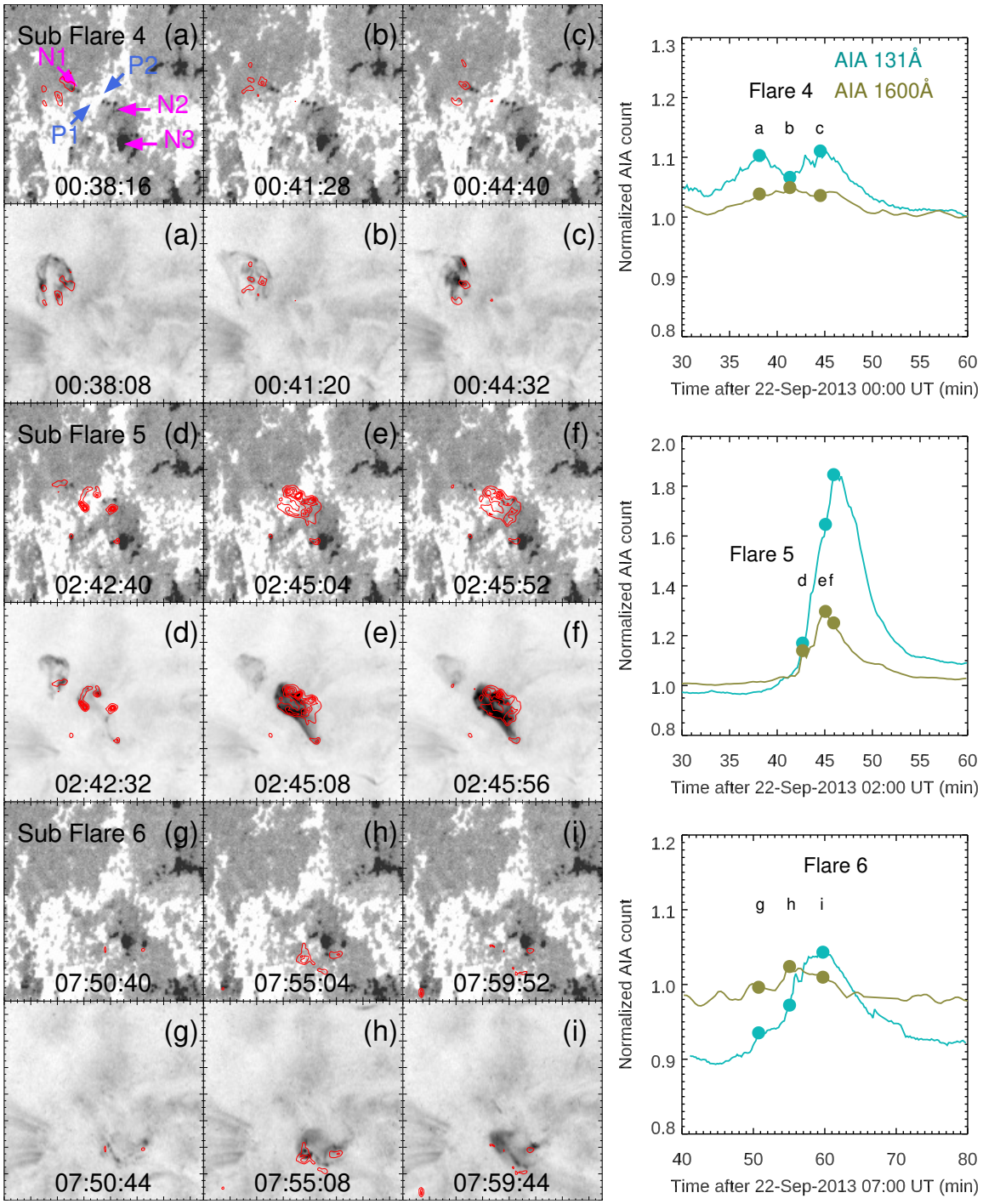

Figure 4. Same as Figure 3, but for subflares 4 to 6.

we found that successive flares resulted in a gradual change of the quadrupolar magnetic configuration, and the gradual migration of the flare kernels to the southwest.

Our results show the similarity of the small flares to the main flare in terms of their magnetic configuration and temporal development, which suggests that the formation process of blobs may be similar to that of the CME. We note that a CME is usually identified with a magnetic flux rope system originating from magnetic reconnection (e.g. Lin & Forbes 2000). Each blob may be regarded as a miniature of a magnetically-detached system (magnetic island or flux rope) like the CME. This leads us to conjecture that the ray may provide only a channel for the blobs to escape from the Sun.

Theoretically, post-CME rays are frequently identified with current sheets, outflows, or slow-mode shocks related to magnetic reconnections that energize electrons and CMEs during the impulsive phases of flares (see the review by Lin et al. 2015) with their lengths

and widths being compared to theoretical values (e.g., Litvinenko 1996; Wood & Neukirch 2005). As pointed out by Kwon et al. (2016), however, post-CME rays are observed much later than the flare impulsive phase and the CME acceleration phase. In the present work, we found that the main flare was followed by successive small flares. Moreover, the locations of these flare kernels gradually changed in time together with the change of the magnetic field configuration. This may imply that the properties of current sheets and rays keep changing because of mutual feedback between the successive flares and the moving features as discussed by Chae et al. (2017). The characteristics of the observed post-CME rays may be the ones that already have been modified by the successive flares.

We emphasize again that all the flares associated with the CME and the blobs occurred not in a simple bipolar configuration, but in a quadrupolar configuration having a curved PIL. This means that the process of producing the blobs as well as the post-CME rays should be understood in three dimensions and as a function of time. In this respect, the observed post-CME rays cannot be considered as a simple edge-on or face-on view of current sheets or magnetic reconnection outflows, but rather the projection of a curtain-shaped structure as proposed by Vršnak et al. (2009). This effect complicates accurate measurements of the width of post-CME rays, implying that their widths cannot be regarded as proxies for those of current sheets.

Acknowledgments

We appreciate the constructive comments by the referees. This research was supported by the National Research Foundation of Korea (NRF-2017R1A2B4004466) and by the Korea Astronomy and Space Science Institute under the R&D program, Development of a Solar Coronagraph on International Space Station (Project No. 2017-1-851-00), supervised by the Ministry of Science, ICT, and Future Planning.

References

Chae, J., Cho, K., Kwon, R.-Y., & Lim, E.-K. 2017, Evidence for a Magnetic Reconnection Origin of Plasma Outflows along Post-CME Rays, ApJ, 841, 49

Forbes, T. G. & Acton, L. W. 1996, Reconnection and Field Line Shrinkage in Solar Flares, ApJ, 459, 330

Ko, Y.-K., Raymond, J. C., Lin, J., et al. 2003, Dynamical and Physical Properties of a Post-Coronal Mass Ejection Current Sheet, ApJ, 594, 1068

Kwon, R.-Y., Vourlidas, A., & Webb, D. 2016, Three-dimensional Geometry of a Current Sheet in the High Solar Corona: Evidence for Reconnection in the Late Stage of the Coronal Mass Ejections, ApJ, 826, 94

Lemen, J. R., Title, A. M., Akin, D. J., et al. 2012, The Atmospheric Imaging Assembly (AIA) on the Solar Dynamics Observatory (SDO), Sol. Phys., 275, 17

Lin, J. & Forbes, T. G. 2000, Effects of Reconnection on the Coronal Mass Ejection Process, J. Geophys. Research, 105, 2375

Lin, J., Ko, Y.-K., Sui, L., et al. 2005, Direct Observations of the Magnetic Reconnection Site of an Eruption on 2003 November 18, ApJ, 622, 1251

Lin, J., Murphy, N. A., Shen, C., et al. 2015, Review on Current Sheets in CME Development: Theories and Observations, Space Sci. Rev., 194, 237

Litvinenko, Y. E. 1996, Particle Acceleration in Reconnecting Current Sheets with a Nonzero Magnetic Field, ApJ, 462, 997

Pesnell, W. D., Thompson, B. J., & Chamberlin, P. C. 2012, The Solar Dynamics Observatory (SDO), Sol. Phys., 275, 3

Riley, P., Lionello, R., Mikić, Z., et al. 2007, "Bursty" Reconnection Following Solar Eruptions: MHD Simulations and Comparison with Observations, ApJ, 655, 591

Savage, S. L., McKenzie, D. E., Reeves, K. K., et al. 2010, Reconnection Outflows and Current Sheet Observed with Hinode/XRT in the 2008 April 9 "Cartwheel CME" Flare, ApJ, 722, 329

Schou, J., Scherrer, P. H., Bush, R. I., et al. 2012, Design and Ground Calibration of the Helioseismic and Magnetic Imager (HMI) Instrument on the Solar Dynamics Observatory (SDO), Sol. Phys., 275, 229

Shen, C., Lin, J., & Murphy, N. A. 2011, Numerical Experiments on Fine Structure within Reconnecting Current Sheets in Solar Flares, ApJ, 737, 14

Vršnak, B., Poletto, G., Vujic, E., et al. 2009, Morphology and Density Structure of Post-CME Current Sheets, A&A, 499, 905

Webb, D. F., Burkepile, J., Forbes, T. G., & Riley, P. 2003, Observational Evidence of New Current Sheets Trailing Coronal Mass Ejections, J. Geophys. Research, 108, 1440

Webb, D. F. & Vourlidas, A. 2016, LASCO White-Light Observations of Eruptive Current Sheets Trailing CMEs, Sol. Phys. 291, 3725

Wood, P. & Neukirch, T. 2005, Electron Acceleration in Reconnecting Current Sheets, Sol. Phys., 226, 73